IEEE Transactions on Nanobioscience

Breast-Cancer Biomarker (C-erbB-2) Detection in Saliva/Serum Based on $In_{1-x}Ga_xAs$/Si Hetero Junction Dopingless TFET Biosensor

Shradhya Singh[1*], Navaneet Kumar Singh[2] and Sangeeta Singh[1], Member IEEE

[1] *Microelectronics & VLSI Lab National Institute of Technology Patna, India*
[2] *Department of ECE, University college of Engineering and Technology (UCET), VBU, Hazaribag, Jharkhand.*
[*] *Member, IEEE*

Abstract—This research article reports the electrical detection of breast-cancer biomarker (C-erbB-2) in saliva/serum based on $In_{1-x}Ga_xAs$/Si heterojunction dopingless tunnel FET (HJ-DL-TFET) biosensor for highly sensitive and real-time detection. The work takes into account the interface charge modulation effect in dopingless extended gate heterostructure TFET with embedded nanocavity biosensors for the precise, reliable, and fast detection of antigens present in the body fluids such as saliva in place of blood serum. The reported biosensor is numerically simulated in 2D using the SILVACO ATLAS exhaustive calibrated simulation framework. For the biomolecule immobilization, the proposed biosensor has a dual cavity engraved beneath the dual gate structure. This improves the control of biomolecules over the source-to-channel tunneling rate, as well as the control over the electrical performance parameters of the proposed biosensor. Here, a numerical model for the C-erbB-2 interface charge equivalent is also developed. The analysis of device sensitivity in both saliva and serum environments for various C-erbB-2 concentrations has been carried out. Our study reveals that III-V $In_{1-x}Ga_xAs$/Si heterojunction with x composition of 0.2 and extended gate geometry provides an increased tunneling probability, improves the gate control to get a higher I_{ON}/I_{OFF} ratio and higher sensitivity. In addition to this, the impact of interface charges corresponding to the different amounts of C-erbB-2 biomarkers on the biosensor sensitivity (in terms of I_{ON}/I_{OFF} ratio) yields higher sensitivity of the order of 10^6.

Index Terms—InGaAs/Si Heterojunction TFET, breast cancer biomarker, c-erbB-2, sensitivity, TCAD, $In_{1-x}Ga_xAs$/Si hetero junction.

I. INTRODUCTION

Biosensing devices are now necessary for the aftermath of the COVID'19 outbreak. Biosensors have shown great potential in the medical diagnostic field. Throughout the globe, there are various types of biosensors developed such as electrochemical, electrical, photonic, optical biosensors, etc. [1]. Among these wide range of electrical detection devices, FET (field-effect transistor) based biosensors have turned out to be the most convenient alternative due to their inherent advantages of higher sensitivity, smaller scaled dimensions, simpler mechanism of transduction, low cost, technological compatibility with CMOS process, controllable electrical response, and reproducibility [2]. The very first FET-based biosensor was invented by P. Bergvel in 1970 [3]. They designed and investigated a biosensor for neurophysiological measurements, and it was ion sensitive FET (ISFET) [4]. For the charged biomolecules ISFETs demonstrated a good sensitivity. Continuous improvements have been carried out since its invention due to this it has emerged as an ideal approach for the fast and accurate detection of various analytes (such as glucose, penicillin, urea, pesticides, phenolic compounds, steroidal glycoalkaloids, creatinine, etc) as well as for drug discovery [5]-[10]. Although these Si-based sensors demonstrated a huge range of sensing regimes varying from macro-scale environmental monitoring [11] to nano-scale studies of biomolecular interactions [12]. Chemical and biological agents, on the other hand, have been found to target and distort Si. Although SiO_2 can ensure sufficient adhesion and adequate growth of living cells. It is being claimed by Cimalla et al. [13] and Kokawa et al. [14] that AlGaN/GaN devices have better biocompatibility and adhesive properties, regardless of the Al mole fraction or the process steps involved. The material performance of these devices with III-V group based materials are better than Si-sensors in reference to the higher thermal and electrical properties than Si-based systems due to its higher strength, chemical stability, higher bandgap, higher chemical stability, quicker responses, and above all their stability in aqueous solutions [15]. Moreover, the advanced functionalities such as high speed, low power consumption, enhanced packing density, etc., can be achieved by the miniaturization of device dimensions. But scaling of CMOS technology has obstructed the progress of the semiconductor industry due to various inevitable problems in terms of various short channel effects (SCEs), more leakage current, high consumption of power and degraded ON-to-OFF current ratio.

To counter these problems an emerging tunnel FET device has been developed due to its ability to withstand the detrimental effects of down scaling and it also offers low leakage current and subthreshold slope (SS) below Boltzmann's limit (<60mV/decade). It has also been reported in the literature that the sensitivity performance metrics of MOSFET-based biosensors are also limited by the degradable SS and higher response time. Hence, TFET based biosensors are expected to overcome these limitations owing to its inherent phenomenon i.e. band-to-band tunneling (BTBT) [16]. As band-to-band tunneling phenomenon leads to reduction of SS below 60mV/decade which makes the device faster and also it operates on low gate voltage which further reduces the power consumption. Meanwhile, dopingless TFETs (DLTFETs) have been reported to ease the fabrication process of TFET as they do not need a costly diffusion or ion implantation process to achieve an ultra-sharp doping profile for the source and drain regions [17]. Hence, owing to the inherent steep SS behaviour of TFET, TFET based biosensors are expected to show higher sensitivity with better response time

Corresponding author: Shradhya Singh (e-mail: shradhyas.phd18.ec@nitp.ac.in)

[18]-[22].

Even though TFET has become a strong alternative to CMOS technology, it suffers from the major limitations of low ON current and ambipolar conduction [23],[24]. To counter these limitations, various new modified TFET structures have emerged, such as hetero-dielectric TFET, multigate TFET, and vertical TFET [20]-[22] etc. Further, to utilize the TFET device for biosensing applications various structures have been proposed for label-free biosensing such as biosensor based on buried strained SiGe source TFET [25], dual-channel trench gate [26], front gate engineered back gate biased DMTFET with front gate engineering and biasing on back gate [27] and hetero gate oxide TFET [28]-[30]. Most of these structures have been found to have either low sensitivity or higher fabrication complexity, which prevents them from being accepted by industries as standard biosensor models.

Furthermore, in recent years, breast cancer has turned out as a serious public health issue due to its high occurrence frequency. By mammography, the majority of patients are screened for breast cancer. This procedure is expensive and invasive too which limits the screening frequency. A work by Michaelson et al. [23] indicates that a patient has a survival rate of 96%, if the patient could be screened every 3 months. Thus, the death rate could be reduced in breast cancer patients by increasing the frequency of screening. Due to the lack of cheap and reliable technology that can detect breast cancer non-invasively, this is not currently possible. C-erbB-2 (also known as HER2, erb-b2 receptor tyrosine kinase 2, ERBB2, NEU, MLN 19, NGL, CD340) is a human epidermal growth factor receptor that can be used to detect breast cancer. During the growth and production of some aggressive types of breast cancer, between 25 to 30% of this transmembrane glycoprotein is overexpressed.

Inspired by these concurrent advancements in the dopingless hetero TFET and urgent need for the breast-cancer detection, the current study reports the electrical detection of breast-cancer biomarker (C-erbB-2) in saliva/serum using an $In_{1-x}Ga_xAs/Si$ heterojunction dopingless TFET (HJ-DLTFET) biosensor for highly sensitive and real-time biosensor. The work considers the interface charge modulation effect in a dopingless extended gate heterostructure TFET with embedded nanocavity biosensors for the precise, accurate, and quick detection of antigens present in body fluids such as saliva rather than blood serum. The III-V heterostructure TFET biosensors can dominate the biomedical lab-on-chip industry in near future. Higher gate control and lower leakage current are two advantages of the proposed extended gate structure. In addition, the length of the extended gates affects the electric field within the channel. For different C-erbB-2 concentrations, system sensitivity has been investigated in both saliva and serum conditions. Our research shows that the III-V $In_{1-x}Ga_xAs/Si$ hetero junction with the x composition of 0.2 and an extended gate geometry increases tunneling probability, improves gate power, and increases sensitivity. Greater flexibility in tunneling rate can be achieved by controlling the dimensions of the extended gate. Due to the box-like gate design, improved I_{ON}, a lower SS and a reduced leakage current can be achieved at the same time [32]-[34]. Moreover, heterostructure TFETs have an additional benefit of a flexible bandgap material at the source/channel interface, which can

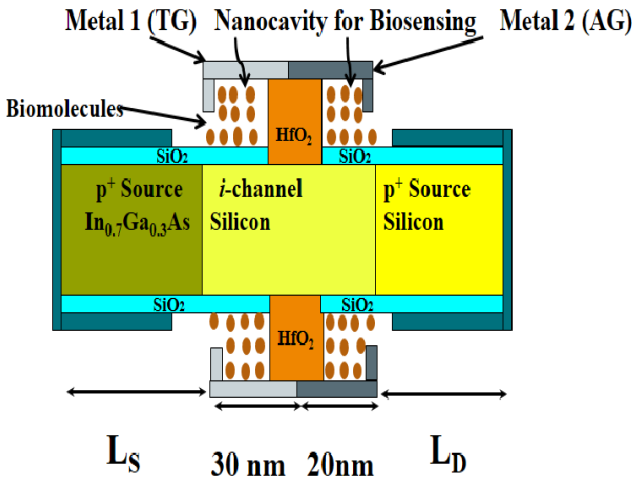

Fig. 1: Proposed device structure of $In_{1-x}Ga_xAs/Si$ heterojunction dopingless TFET sensor for C-erbB-2 detection.

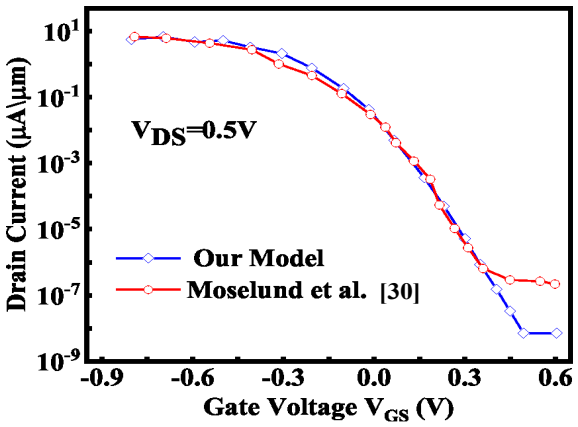

Fig. 2: Calibration of the proposed simulation model against the experimental data in [30].

be used to regulate the tunneling rate. Because of these benefits, HJ-DLTFET is a viable device option for biosensing applications [35]-[41]. Our study claims that it is a potential candidate for mass production because of its high sensitivity in terms of I_{ON}/I_{OFF} current ratio, improved SS, and easier fabrication steps because of hetero-epitaxial techniques such as selective area growth (SAG) [42].

This work is organized as follows: The reported biosensor structural parameters, material, and doping are all explained in Section II. Section III covers the C-erb-2 modeling in depth. Then the electrostatic analysis as well as sensitivity analysis $In_{1-x}Ga_xAs/Si$ heterojunction dopingless TFET biosensor are investigated in Section IV. Finally, Section V outlines the conclusions of research work.

II. DEVICE STRUCTURE AND SIMULATION METHODOLOGIES

The 2-D schematic of the proposed device HJ-DLTFET based biosensor with dual nanocavity underneath of gate electrode is shown in Fig. 1. The proposed structure is utilized for the sensitivity analysis of the breast cancer biomarkers i.e. C-erbB-2

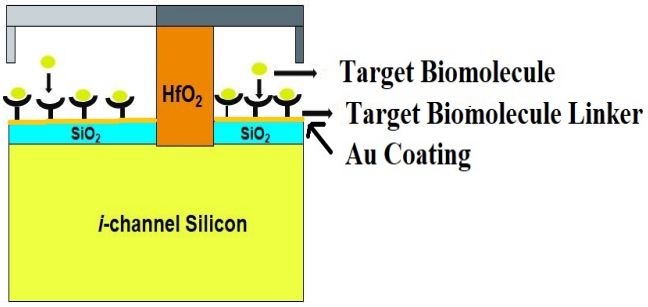

Fig. 3: Bio-immobilization at the functionalized cavity region in HJ-DLTFET.

Table 1: Simulation parameters for $In_{1-x}Ga_xAs$/Si heterojunction dopingless TFET biosensor.

Parameters(Symbols)	$In_{1-x}Ga_xAs$/Si HJ-DLTFET Biosensor
Silicon thickness (T_{Si})	10 nm
Gate-oxide thickness (T_{ox})	2 nm
Gate length (L_G)	50 nm
Source length (L_S)	100 nm
Drain length (L_D)	100 nm
Background doping (N_{in})	$1 \times 10^{16} cm^{-3}$
Source work-function (ϕ_S(Pt))	5.93 eV
Drain work-function (ϕ_D (Hf))	3.9 eV
Gate Dielectric constant (ϵ_{ox})	HfO_2 (22)
Source material	$In_{1-x}Ga_xAs$
Channel Material	Si
Drain Material	Si
Metal1	Aluminium (ϕ_1=3.8 eV)
Metal2	Aluminium (ϕ_2=4.8 eV)

protein. TFET heterostructures provide greater flexibility such as the formation of the depletion region at the junction, controlling the band-to-band tunneling (BTBT), the effective mass of the carrier, lowers SS, and optimizes both leakage and ON-state currents simultaneously [42]-[45]. In the proposed HJ-DLTFET structure, source-side material is chosen as $In_{1-x}Ga_xAs$ with Ga mole fraction of x = 0.2. The considered heterostructure has an 8% lattice mismatch and has a lower leakage current than InAs/Si HTFET [30]. Further, $In_{1-x}Ga_xAs$ shows widely tunable band gaps, high electron mobilities, tunable Schottky barrier heights, and the overall reduced lattice mismatch restrictions and also the formation of low-defect density heterostructure devices [46].

The major benefit of choosing this material towards the source side is in terms of enhanced tunneling rate as well as ON current owing to its low effective mass and lower band gap. To control leakage current and to achieve an abrupt band bending towards the source-channel junction, silicon is used for both the channel and the drain regions. It leads to an improvement in the electric field at the junction. Here, the source (p^+) and drain (n^+) regions have been created by dopingless technique [17], by selecting the suitable metal work-function on either sides of source and drain electrodes as 5.93 eV and 3.9 eV, respectively. Further, there are two different metals that are used as gate metal gate; Aluminum (ϕ_1=3.8 eV) towards the source side of length 30 nm and Copper (ϕ_2=4.8 eV) towards the drain side of length 20 nm for achieving improved SS and reduced leakage current. To improve the gate control over channel extended tunneling gate (TG) is introduced towards source-channel junction due to an increase in the electric

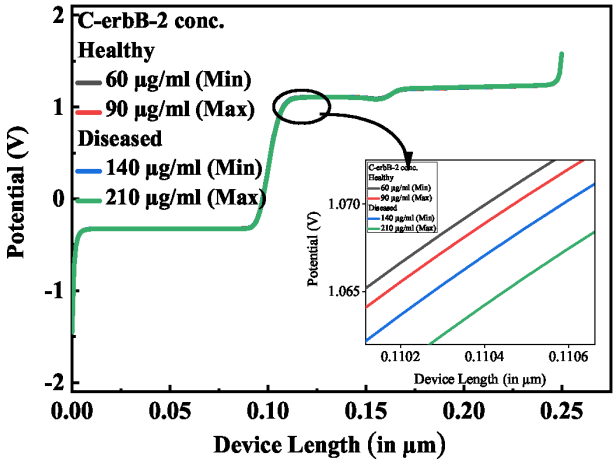

Fig. 4: Channel potential profile for boundary concentrations of C-erbB-2 in serum of healthy and diseased sample.

field and auxiliary gate (AG) towards the drain-channel junction controls the thermionic emission current. The binding site cavity for the protein of interest has been created underneath the gate electrode, which has been bifurcated into 20 nm at source channel junction and 10 nm at drain-channel junction. HfO_2 is utilized as gate dielectric and a thin SiO_2 layer is used as a passivation dielectric for biomolecules. Biomolecules are considered to be 100 % pure and free of contamination for biosensing applications. In general, the cavity is expected to be fully filled with biomolecules.

To investigate the device characteristics and to analyze the device sensitivity, the device is simulated using the SILVACO ATLAS TCAD tool [47]. The tunneling rate at the junctions is computed using a dynamic non-local band-to-band tunneling model. The mobility degradation effect is introduced using a high field-dependent and doping-dependent mobility model. The drift-diffusion transport model, the Shockley-Read-Hall recombination/generation model, and the Auger recombination/generation model are all taken into account. For accuracy, Fermi-Dirac statistics and a bandgap narrowing models are used. For the calibration and validation of the deployed simulation model authors have used Moselund et al. frame work [30] as shown in Fig. 2. Since experimental data for InGaAs/Si n-type TFET is not available, the calibration is carried out for InAs/Si-TFET of the lateral p-type. The structure dimensions are as per the dimension in [30], but since for this simulation interface traps are not taken into account, hence lower leakage current than experimental values (Fig. 2) can be observed in the simulation results. To predict the corresponding charge/potential produced when 1 vial (5μg/ml) sample of the diseased one (which is applied at the gate underneath the cavity region), a numerical model for C-erbB-2 oncoprotein concentration in human saliva and serum is developed. It can be used to model the other antigens or proteins using its concentration and molecular mass in diseased as well as normal states. All the device parameters considered for the device simulation are listed in Table. 1.

III. C-ERBB-2 MODEL

Breast cancer has become a serious public health issue in recent years due to its high level of occurrence. C-erbB-2 (also known

Table 2: Range of C-erbB-2 concentrations in human saliva and serum for a healthy and a diseased person

C-erbB-2 concentration	In Saliva				In Serum			
	Healthy		Diseased		Healthy		Diseased	
	Min	Max	Min	Max	Min	Max	Min	Max
Clinically relevant concentration (μ g/ml) [40]	4	6	9	13	60	90	140	210
Equivalent interface charge,Q_{BM} ($\times 10^{14}/m^2$)	-0.63	-0.948	-1.42	-2.05	-9.47	-14.20	-22.11	-33.10

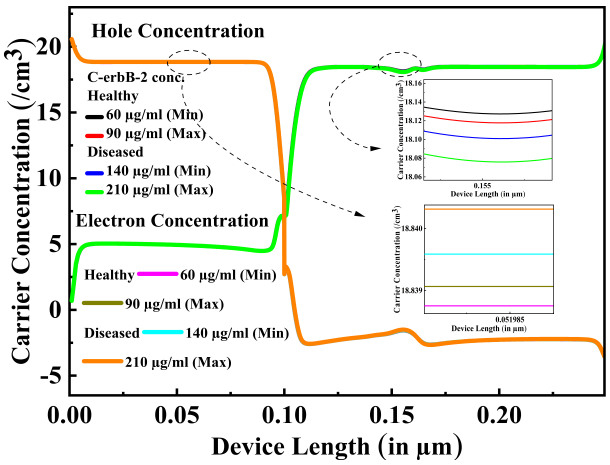

Fig. 5: Carrier concentration profile for boundary concentrations of C-erbB-2 in serum of healthy and diseased sample.

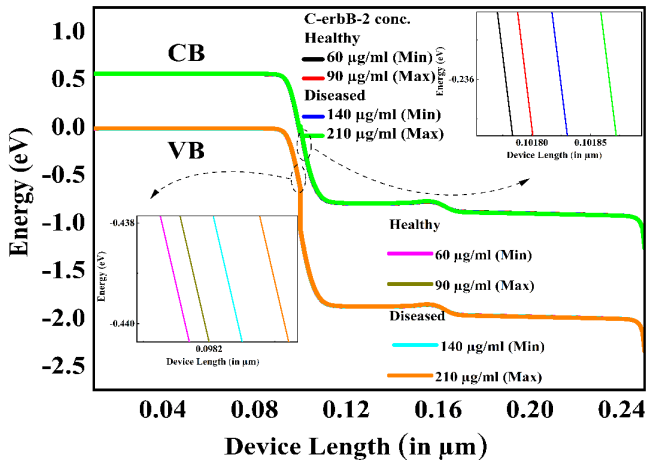

Fig. 6: Energy band diagram for boundary concentrations of C-erbB-2 in serum for a healthy and a diseased sample.

as ERBB2, HER2, erb-b2 receptor tyrosine kinase 2, NEU, MLN 19, NGL, CD340) is a human epidermal growth factor receptor that can be used to detect breast cancer. During the production of some aggressive breast cancer types, this trans-membrane glycoprotein is over expressed by 25 to 30% [35], [36].

Here, for the very first time, $In_{1-x}Ga_xAs/Si$ heterojunction dopingless TFET has been utilized for the detection of C-erbB-2 oncoprotein. The anchoring of the antigen to its individual functionalized antibody in the area of the cavity coated with SiO_2 is the part of the physical recognition process. The detection procedure consists of a thin layer of self-assembled thioglycolic acid that serves as the target biomolecule linker in this case ($HSCH_2COOH$) as shown in Fig. 3. Thiol and gold coated SiO_2 molecular linking causes self-assembly. Here, a strong contact between gold and the thiol group of the thioglycolic acid has been used to attach a self-assembled monolayer of thioglycolic acid, $HSCH_2COOH$, an organic molecule comprising both a thiol mercaptan and a carboxylic acid functional group, on the Au surface in the cavity area.This device initially put in an ozone/UV chamber before being immersed in a 1 mM thioglycolicacid aqueous solution at ambient temperature. The thioglycolic acid is binded to the Au surface at the cavity region, leaving the COOH groups open for chemical linkage of other functional groups. Before real-time measurement of c-erbB-2 antigen, the device was incubated in a phosphate-buffered saline (PBS) solution of 500 lg/ml c-erbB-2 monoclonal antibody for 18 hours [48],[49]. Charge control or voltage-driven models may be designed to analyse the device's sensing behavior, and the equivalent charge due to biomarker C-erbB-2 must be numerically modeled. This is accomplished by calculating the effective net charge due to C-erbB-2 molecules in saliva as well as serum and applying it as an interface charge into the nano-cavity region for biomarkers to be detected. 4-6 μg/ml concentrations of C-erbB-2 in saliva at pH value 7.3 and 60-90μg/ml in serum at pH value 7.35 are clinically significant for healthy person. Cancer patients have elevated levels of concentration 9-13 μg/ml in saliva and 140-210 μg/ml in serum [35],[36]. The net charge per 1M is determined by multiplying the molar concentration of the protein by the charge in a single molecule [50]. After multiplying 1M by the Avogadro's number of particles, the net charge equivalent of C-erbB-2 can be computed as [51].

$$Q_{BM} = (conc.of BM \times q_{BM})\, AvogadroNumber \qquad (1)$$

where, q_{BM} represents the effective charge on individual protein molecule (biomarker). Q_{BM} represents the net charge of C-erbB-2 and Avogadro's Number is 6.023×10^{23}. The effective interface charge due to C-erbB-2 immobilized in the cavity region falls in the range 10^{14}-$10^{15}/m^2$ (Table. 2). To simulate the impact of the presence of biomolecule in the cavity region on the device characteristics, the cavity region underneath gate electrode is initially considered as empty i.e. filled with air permittivity and for this condition the drain current is plotted for the device which becomes the reference current to analyze the device sensitivity. Then, it is expected that the biomaker C-erbB-2 gets filled in the entire nanocavity, then the drain current is computed and calibrated to detect the presence of the biomarker in the sample. Alternatively, as C-erbB-2 is a charged molecule, hence their immobilization in the cavity regions also alters the flat band voltage. Thus, this change in the flat-band voltage (as shown in eqn. (2)) could also be deployed for the breast cancer detection.

IV. RESULTS AND DISCUSSIONS

In this section, the sensitivity of the proposed device HJ-DLTFET based biosensor for different concentrations of the targeted biomarker C-erbB-2 molecules in saliva and serum of the healthy and diseased persons have been investigated. The analysis of the device has been accomplished by calculating the effective charge due to the presence

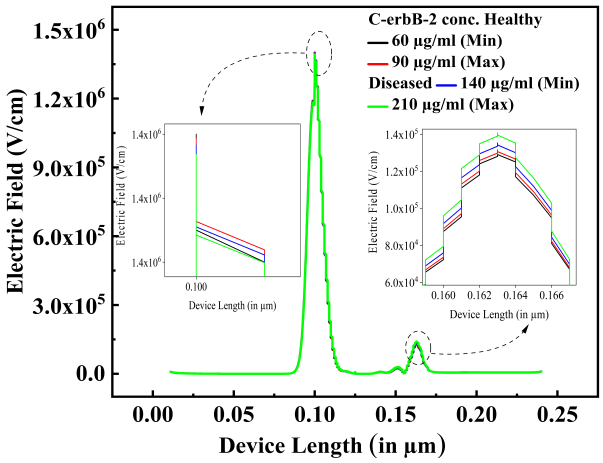

Fig. 7: Electric field distribution for the boundary concentrations of C-erbB-2 in serum for healthy and diseased.

of C-erbB-2 molecules in saliva and serum and applying it as an interface charge of the device. The corresponding interface charges of the immobilized biomarkers are mentioned in Table. 2.

A. Electrostatic analysis of HJ-DLTFET Based Biosensor

The channel potential in the nano-cavity region underneath the gate electrode falls with the variation of negatively charged C-erbB-2 in the cavity region. The variation of channel potential for different concentrations in the serum is plotted in Fig. 4. It can be noted that the channel potential reduces by 5mV-10mV when peak C-erbB-2 concentration in serum for diseased state is taken into the test. The change in channel potential is achieved due to the variation in the flat band voltage i.e. directly proportional to the applied interface charge. The change in flat band voltage can be expressed as eqn. (2) [52]:

$$\Delta V_{FB} = \frac{Q_{BM}}{C_{gate}} \tag{2}$$

where, V_{FB} denotes the flat band voltage, C_{gate} stands for the gate capacitance, and Q_{BM} represents the net charge of C-erbB-2. The carrier concentration variations in all three source, channel and drain regions of the device (1 nm below the oxide interface) is shown in Fig. 5. It can be observed that by utilizing the concept of dopingless technique, both hole as well as the electron concentrations are induced of the order of $10^{18}/cm^3$ (even without actual metallurgical doping) for all the concentrations of C-erbB-2 immobilized in the cavity region. The electron concentration in the channel region is lower for higher C-erbB-2 concentration in the cavity region corresponds to its high negative interface charge results in lower tunneling rate. The energy band diagrams of the proposed device for different concentrations of serum corresponds to the healthy and diseased person is shown are Fig. 6. It can be noticed that an increased serum concentration in diseased persons reduces the band bending that leads to a lower tunneling rate. Splitting of the cavity underneath the gate electrode reduces the change in the effective capacitance due to the immobilized biomarkers into the nanocavity region. At the source-channel junction the band bending is largest as compared to other areas due to extended TG [42], the conduction band bends under Fermi level (E_F) and the interband tunneling gap becomes less with the effect of applying gate bias for which the rate of the band to band tunneling increases exponentially [50],[51]. As the interband tunneling region enhances with the introduction of a higher concentration of serum at the binding site, the tunneling rate reduces. It can be understood with the expression in eqn. (3) [53]:

$$log(T) \propto -\sqrt{m^* E_g}\lambda_{Tun} \tag{3}$$

here, m^* denotes the tunneling charge effective mass, λ_{Tun} is the tunneling length, E_g is the energy bandgap of the heteromaterial, and T represents the tunneling probability. Fig. 7 shows the electric field variation at source/channel junction for the different concentrations of C-erbB-2 immobilized in cavity region. The highest electric field of the order of 10^6 has been achieved due to the extended TG, which results in enhanced BTBT rate at the source-channel junction that leads to the highest ON current. Due to the exponential dependence of tunneling length on BTBT rate, surface potential as well as electric field reduces for a higher concentration of biomarkers as evident from eqn. (3).

Fig. 8 shows the drain current variation with the modulation of the gate potential in response to the biomarkers interaction in comparison to the air in the cavity. The depletion width modulation takes place in the channel region near the conducting edge due to the concentration of C-erbB-2 exposed into the cavity region. In the C-erbB-2 biomarker model for the device design, interface charge at the oxide-channel interface gets modulated depending upon the serum and saliva concentrations of healthy and diseased persons. When an increased bio charge is applied, the depletion width region increases, which leads to a decrease in the current flow. Therefore, the change in current increases as the concentration of charged target biomolecules increases. In short, it has the same effects as the application of negative bias to the gate electrode. For the concentrations of C-erbB-2 in saliva, it can be observed that the simulation results show less variation from Fig. 8 (a) however as the C-erbB-2 concentration increases in saliva this variation in the drain current between the device filled with biomolecules and with air in Fig. 8 (b) become significant datum owing to the enhancement in the corresponding interface charges.

Fig. 9 (a)-(d) show the potential distribution contours for the different concentration of C-erbB-2 biomarker in serum of healthy and diseased person. It is evident from these contours that the potential distribution in channel region is significantly reduced as the C-erbB-2 concentration increases, this leads to a reduction in the electric field for higher C-erbB-2 concentrations, which lowers the ON current.

Fig. 10(a)-(d) depict a detailed study of the device performance parameters in terms of I_{ON}, I_{OFF}, I_{ON}/I_{OFF} ratio, and SS for the serum concentrations of healthy as well as the diseased person immobilized in the cavity region. It is observed from the figure that ON current reduces negligibly with the concentration variation and OFF current also reduces and achieves a value as 10^{-17} A/μm for the diseased person. Therefore ON-to-OFF current ratio increases and reaches to the value of 1.2 $\times 10^{12}$ in diseased concentration which is almost double as compared to the serum concentration of healthy person. The SS has been achieved as 27 mV/decade almost for each concentration. Fig. 11 (a)-(d) represent all the performance parameters of the proposed structure in terms of I_{ON}, I_{OFF},

This article has been accepted for publication in a future issue of this journal, but has not been fully edited. Content may change prior to final publication. Citation information: DOI 10.1109/TNB.2021.3139345, IEEE Transactions on NanoBioscience

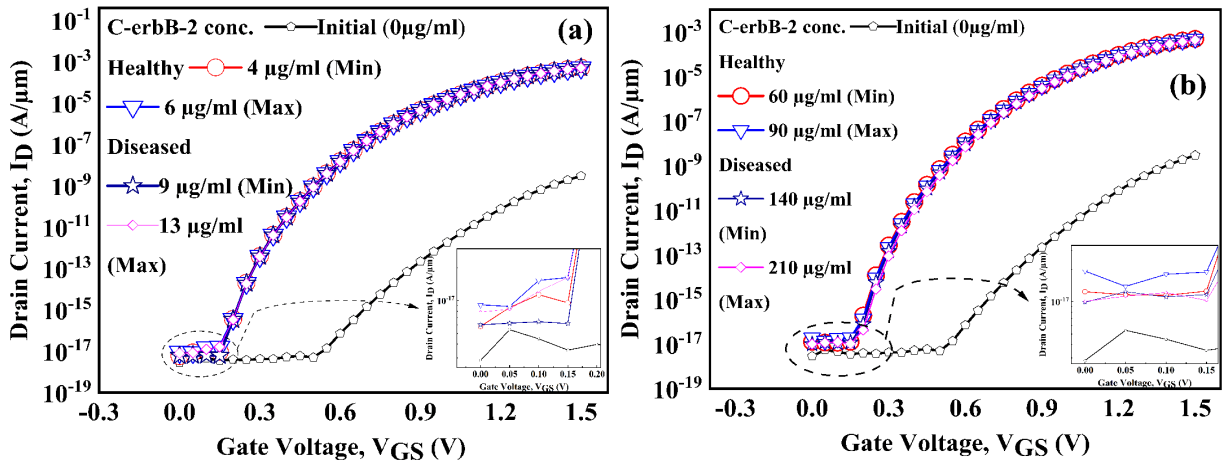

Fig. 8: Transfer characteristics for boundary concentrations of C-erbB-2 in (a) saliva of healthy and diseased and (b) serum of healthy and diseased.

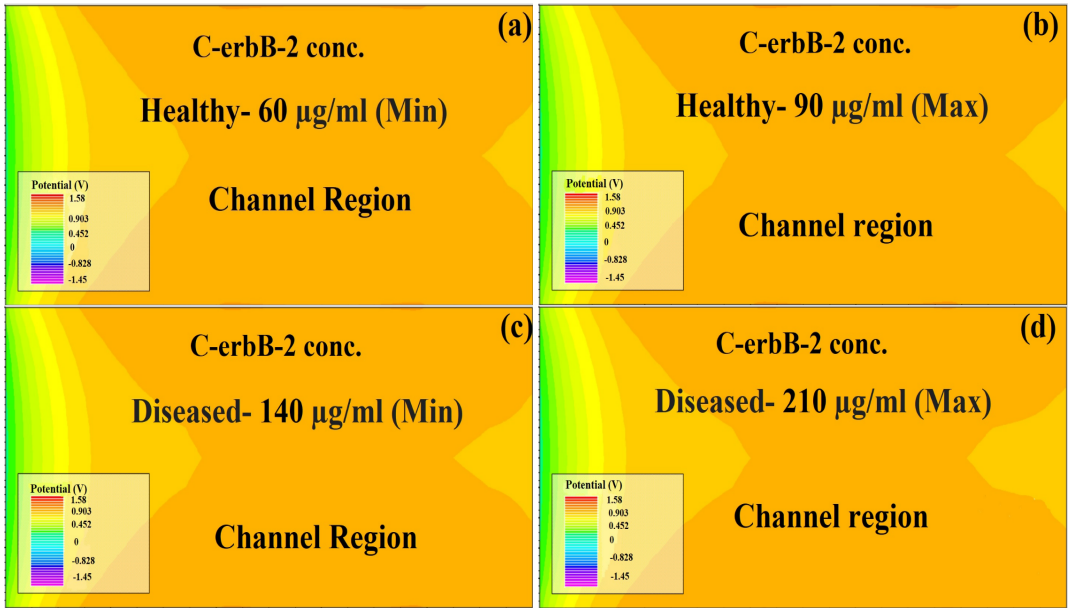

Fig. 9: Potential contour for serum (a) healthy 60 μm/ml (Min.), (b) healthy 90 μm/ml (Max.), (c) diseased 140 μm/ml (Min.), and (d) diseased 210 μm/ml (Max.).

Table 3: Impact of mole fraction variation on I_{ON}/I_{OFF} ratio and sensitivity for range of C-erbB-2 concentrations in human serum of healthy and diseased person.

CerbB-2 concentration		In Serum			
		Healthy		Diseased	
Mole Fraction	Parameters	Min	Max	Min	Max
x=0.1	I_{ON}/I_{OFF}	7.85×10^{10}	7.45×10^{10}	6.98×10^{10}	6.29×10^{10}
	Sensitivity	7.29×10^{5}	7.64×10^{5}	6.11×10^{5}	5.62×10^{5}
x=0.2	I_{ON}/I_{OFF}	2.6×10^{12}	2.51×10^{12}	1.91×10^{12}	1.63×10^{12}
	Sensitivity	3.96×10^{6}	3.81×10^{6}	2.91×10^{6}	2.48×10^{6}
x=0.3	I_{ON}/I_{OFF}	4.79×10^{11}	5.02×10^{11}	4.01×10^{11}	3.69×10^{11}
	Sensitivity	7.29×10^{5}	7.64×10^{5}	6.11×10^{5}	5.62×10^{5}
x=0.5	I_{ON}/I_{OFF}	2.54×10^{11}	4.29×10^{11}	2.91×10^{12}	3.05×10^{11}
	Sensitivity	3.86×10^{5}	6.52×10^{5}	4.43×10^{6}	4.63×10^{5}
x=0.7	I_{ON}/I_{OFF}	1.30×10^{10}	2.30×10^{10}	7.84×10^{9}	7.07×10^{9}
	Sensitivity	1.98×10^{4}	3.50×10^{4}	1.19×10^{4}	1.07×10^{4}
x=0.9	I_{ON}/I_{OFF}	3.21×10^{8}	2.77×10^{8}	2.05×10^{8}	1.62×10^{8}
	Sensitivity	4.88×10^{2}	4.21×10^{2}	3.12×10^{2}	2.47×10^{2}

Table 4: Comparison of proposed device with InAs/Si TFET for on I_{ON}/I_{OFF} ratio and sensitivity for range of C-erbB-2 concentrations in human serum of healthy and diseased person.

CerbB2 concentration	Proposed Device (HJ-DLTFET)				InAs/Si TFET [22]			
	Healthy		Diseased		Healthy		Diseased	
Parameters	Min	Max	Min	Max	Min	Max	Min	Max
I_{ON}/I_{OFF}	2.6×10^{12}	2.5×10^{12}	1.9×10^{12}	1.6×10^{12}	5.27×10^{9}	5.74×10^{9}	5.76×10^{9}	5.78×10^{9}
Sensitivity	3.96×10^{6}	3.81×10^{6}	2.9×10^{6}	2.48×10^{6}	2.11×10^{5}	2.29×10^{5}	2.3×10^{5}	2.31×10^{5}

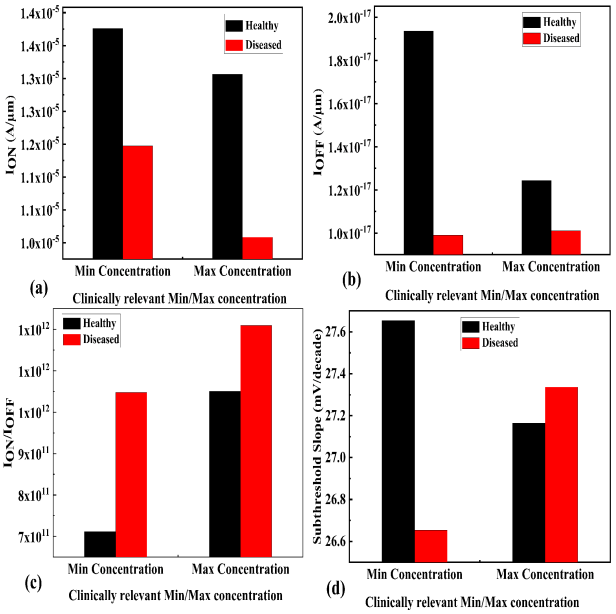

Fig. 10: Performance parameters (a) I_{ON}, (b)I_{OFF}, (c) I_{ON}/I_{OFF} ratio, and (d) SS of the device for boundary concentrations of C-erbB-2 in serum of healthy and diseased persons.

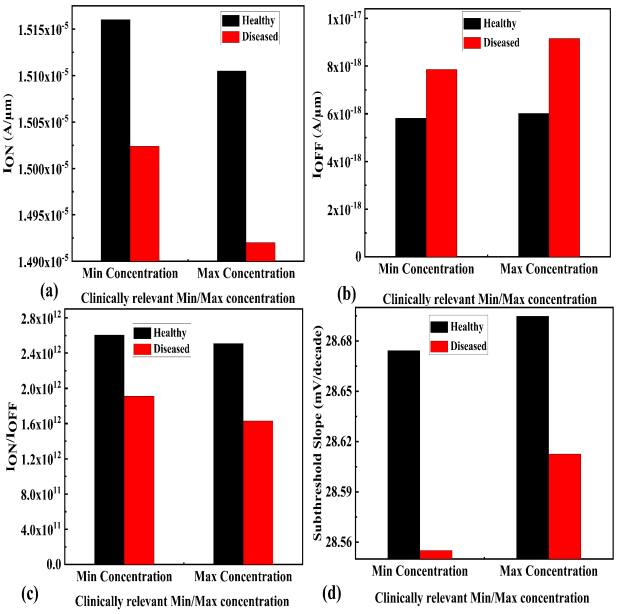

Fig. 11: Performance parameters (a) I_{ON}, (b) I_{OFF}, (c) I_{ON}/I_{OFF} ratio and (d) SS of the device for boundary concentrations of C-erbB-2 in saliva for healthy and diseased persons.

I_{ON}/I_{OFF} ratio, and SS for the saliva concentrations of healthy as well as the diseased person immobilized in the cavity region. It

Table 5: Comparative performance analysis of the reported biosensor with the biosensor state-of-art.

S.N.	Biosensor based on FET	Approximate Sensitivity
1	DM FET (L_{gap}=200 nm) [56]	1×10^{4}
2	DM FET (L_{gap}=100 nm) [56]	3×10^{4}
3	Short Gate DM TFET [57]	1×10^{6}
4	Lateral DM TFET [54]	10
5	Vertical DM TFET [54]	40
6	Nanowire TFET [58]	9×10^{3}
7	Buried strained $Si_{1-x}Ge_x$ DGTFET [25]	2.6×10^{5}
8	DG TFET [55]	1.02×10^{2}
9	Dual Metal Gate SiGe pocket Vertical TFET [55]	2×10^{6}
10	HJ-DLTFET (This work)	3.96×10^{6}

can be noted that the ON current of HJ-DLTFET in presence of biomolecules is the same as 15 μA, for each concentration however the OFF current is 1.5 $\times$ more for the saliva of diseased person as compared to the healthy one. Therefore, I_{ON}/I_{OFF} ratio decreases with an increase in the diseased concentration of C-erbB-2 in saliva. It is of the order of 10^{12} and it gets halved for diseased person as compared to a healthy one. The SS has been achieved as 28.6 mV/decade almost for each concentration. Fig. 12 indicates the impact of concentration of C-erbB-2 biomolecules of saliva and serum in the cavity region on the RF parameter i.e. transconductance (g_m) of the proposed devices. It is defined as $g_m = dI_D/dV_{GS}$. The variation in g_m is almost negligible as an impact of saliva concentration in the cavity region as the corresponding interface charges for the range of concentration is almost similar. This variation is somewhat significant due to serum concentration and the maximum peak value of transconductance is achieved of the order of 1.5×10^{-5} s/μm as depicted in Fig. 12(b).

B. Sensitivity of HJ-DLTFET based biosensor

It is evident from Fig. 8 that the drain current of the proposed device decreases linearly in proportion to the target biomarker concentration immobilized in the cavity region. Hence, the sensitivity of the device to detect C-erbB-2 can be measured as the absolute change in I_{ON}/I_{OFF} ratio per unit increment in the concentration of the C-erbB-2 biomarker in saliva and serum for diseased and healthy person. Fig. 13 shows the sensitivity of the device in terms of I_{ON}/I_{OFF} ratio for the different concentrations of C-erbB-2 in saliva and serum. It can be noticed that the maximum value of the sensitivity of the device achieved is of order 10^6 per μg/L in C-erbB-2 concentration with respect to the absence of biomolecules (air). The sensitivity of the biosensor with respect to air can be measured as [41] eqn. (4):

$$S_{I_{ON}/I_{OFF}} = \frac{S_{I_{ON}/I_{OFF}}(BM)}{S_{I_{ON}/I_{OFF}}(Air)} \quad (4)$$

where, $S_{I_{ON}/I_{OFF}}$(BM) represents the I_{ON}/I_{OFF} ratio of the device immobilized with the biomarkers (C-erbB-2).

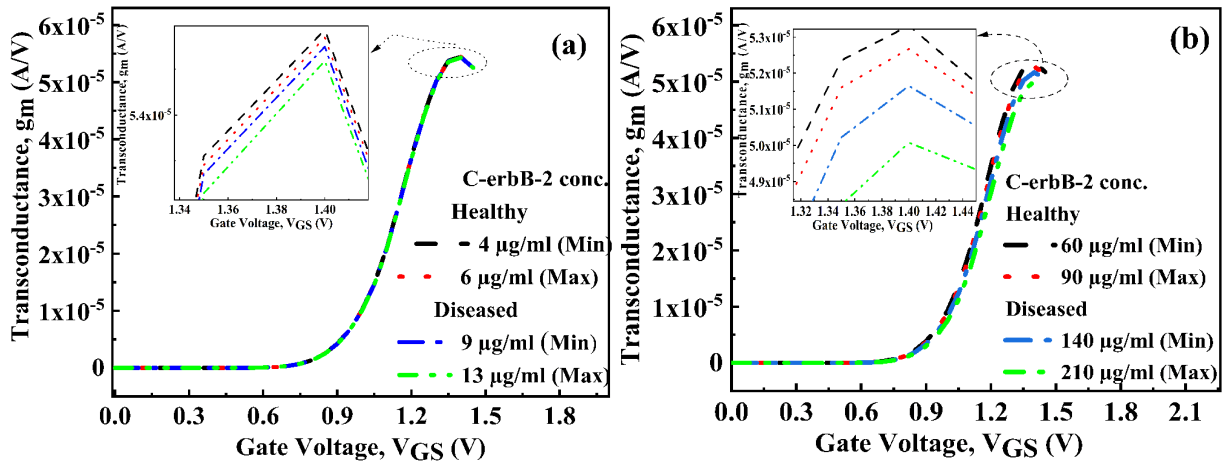

Fig. 12: Transconductance for boundary concentrations of C-erbB-2 in (a) saliva of healthy and diseased persons and (b) serum of healthy and diseased persons.

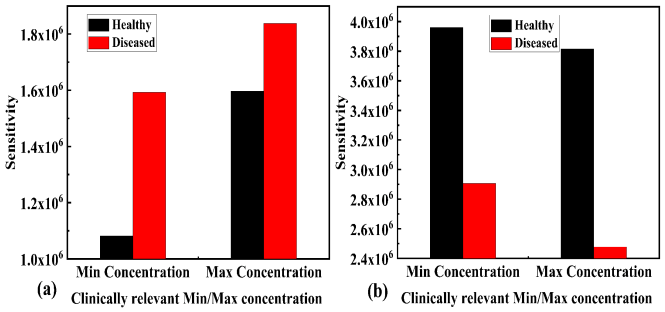

Fig. 13: Sensitivity for boundary concentrations of C-erbB-2 in (a) saliva for healthy and diseased, and (b) serum for healthy and diseased.

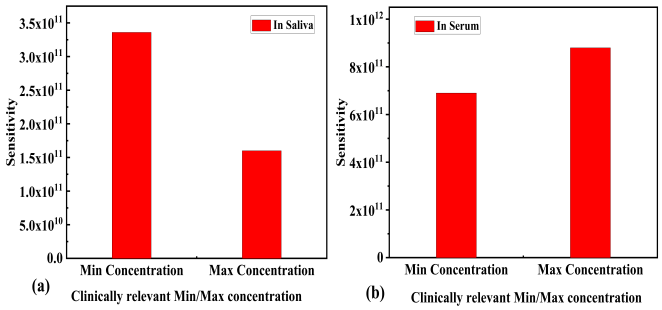

Fig. 14: Sensitivity with respect to healthy sample for boundary concentrations of C-erbB-2 in (a) saliva of diseased (b) serum of diseased.

Further, the sensitivity is also measured for the diseased sample with respect to healthy sample by evaluating the difference between I_{ON}/I_{OFF} ratio of diseased sample and I_{ON}/I_{OFF} ratio of healthy sample. Fig. 14 (a) and (b) represent the sensitivity for the minimum and the maximum concentration boundaries of saliva and serum, respectively. It can be noticed that the sensitivity of the serum based sample is enhanced in comparison to saliva based sample. Table. 3 depicts the I_{ON}/I_{OFF} ratio for various mole fractions of Gallium in $In_{1-x}Ga_xAs$/Si heterojunction source-channel interface for the diseased and healthy state concentration of C-erbB-2 in serum. Furthermore, the reduction in the Ga mole fraction leads to an increment in the tunneling rate and therefore improves the ON

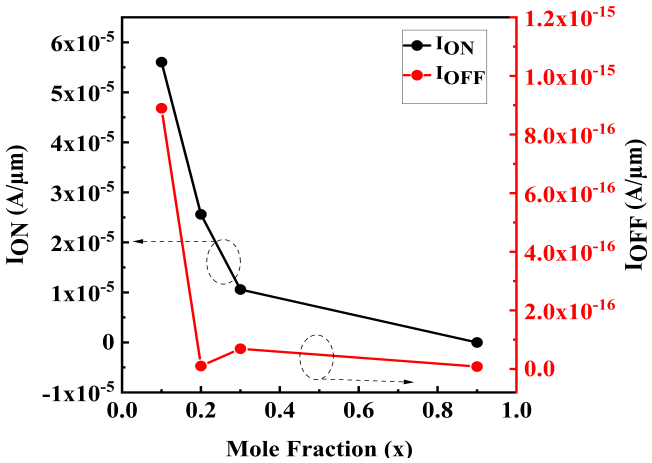

Fig. 15: Variation of ON current and OFF current for different mole fractions of Ga in HJ-DLTFET based biosensor.

current and also improves the I_{ON}/I_{OFF} ratio. However, the shift of I_{ON}/I_{OFF} ratio and the sensitivity of the proposed device to detect the target biomarker is maximum for the mole fraction as 0.2; the amount of shift of I_{ON}/I_{OFF} ratio for different concentrations are less at x = 0.1,0.3,0.5,0.7 and 0.9 in comparison to x = 0.2, which depends on the shift in surface potential and the overall band bending [45]. Due to this with the reduction of mole fraction (x) causes an increase in I_{ON} and I_{OFF} current both as depicted in Fig. 15. It is noted here that I_{ON} current get almost double for x = 0.1 as compared to x = 0.2 but leakage current increases almost 90 ×. This leads a degradation in I_{ON}/I_{OFF} current ratio as x decreases from 0.2 to 0.1, which is also mentioned in Table. 3. Therefore, mole fraction x = 0.2 is considered as the optimum value Ga. Table. 4 illustrates the comparison of the proposed device with InAs/Si TFET structure. It can be observed that proposed $In_{1-x}Ga_xAs$/Si heterojunction dopingless TFET (HJ-DLTFET) shows better performance as compared to InAS/Si in terms of I_{ON}/I_{OFF} ratio and sensitivity parameters. Further, the comparison of proposed structure with other previously reported biosensors is illustrated in Table. 5. It is evident that the proposed $In_{1-x}Ga_xAs$/Si heterojunction dopingless TFET (HJ-DLTFET) that shows better sensitivity and flexibility in designing. The major advantage of the

present manuscript is to its ultralow power applications as compared with the earlier reported HEMT based biosensors to detect breast cancer. Further, owing to the dopingless structure considered, the fabrication process also gets easier and thermal budget also gets reduced with an inherent resilience towards the random dopants fluctuations (RDFs).

V. CONCLUSION

In this work, breast cancer biomarker, C-erbB-2 detection has been investigated based on the proposed $In_{1-x}Ga_xAs/Si$ heterojunction dopingless TFET structure. This study considers the interface charge modulation effect in a dopingless extended gate heterostructure TFET with embedded nanocavity biosensors for the accurate, effective, and quick detection of antigens in body fluids other than blood serum. The addition of TG/AG and extended gate improves the device I_{ON}/I_{OFF} ratio as well as the device sensitivity. The impact of biomarker immobilization at the binding sites on the drain current, channel potential, electric field, I_{ON}/I_{OFF} ratio, and channel transconductance has been studied by incorporating the model for different concentrations of C-erbB-2 biomarker in human saliva and serum of the healthy and diseased person. The I_{ON}/I_{OFF} ratio has been utilized as the major sensing metric throughout the work. The range of sensing I_{ON}/I_{OFF} ratio for diseased and healthy state concentration of C-erbB-2 in saliva and serum has been investigated along with the impact of mole fraction (x) variation in $In_{1-x}Ga_xAs$ on device sensitivity. A better sensitivity has been achieved at lower mole fraction of 0.2 and for the extended gate geometry. This investigation pledges for the potential of this structure for the array-based screening and diagnosis of C-erbB-2, and additional advantages are simpler mechanism of transduction, low cost, technologies compatibility with CMOS process, controllable electrical response, and reproducibility.

REFERENCES

[1] P. Mehrotra, "Biosensors and their applications-A review", *J Oral Biol Craniofac Res.*, vol. 6, no. 2, pp. 153–159, May 2016.

[2] L. Syedmoradi, A. Ahmadi, M.L. Norton, K. Omidfar, "A review on nanomaterial-based field effect transistor technology for biomarker detection", *Microchim. Acta*, vol. 186, no. 11, pp. 1-23, Nov. 2019.

[3] P. Bergveld, "Development of an ion-sensitive solid-state device for neurophysiological measurements", *IEEE. Trans. Biomed. Eng.*, no. 1, pp. 70-71, Jan. 1970.

[4] P. Duroux, C. Emde, P. Bauerfeind, C. Francis, A. Grisel, L. Thybaud, D. Arstrong, C. Depeursinge, A.L. Blum, "The ion sensitive field effect transistor (ISFET) pH electrode: A new sensor for long term ambulatory pH monitoring", *Gut*, vol. 32, no. 3, pp. 240-245, Mar. 1991.

[5] A.V. Rebriiev, N.F. Starodub, "Enzymatic Biosensor Based on the ISFET and Photopolymeric Membrane for the Determinaion of Urea", *Electroanalysis*, vol. 16, no. 22, pp. 1891-1895, Nov. 2004.

[6] A. Poghossian, M.J. Schöning, P. Schroth, A. Simonis, H. Lüth, "An ISFET-based penicillin sensor with high sensitivity, low detection limit and long lifetime", *Sens. Actuat. B*, vol. 76, no.1-3, pp. 519–526, Jun. 2001.

[7] A.L. Simonian, A. Flounders, J. Wild, "FET-based biosensors for the direct detection of organophosphate neurotoxins", *Electroanalysis (N.Y.N.Y.)*, vol. 16, no. 22, pp. 1896–1906, 2004.

[8] A.L. Simonian, J.K. Grimsley, A.W. Flounders, J.S. Schoeniger, T.C. Cheng, J.J. DeFrank, J.R. Wild, "Enzyme based biosensor for the direct detection of fluorine containing organophosphates", *Anal. Chim. Acta*, 442, vol. 1, pp. 15-23, Aug. 2001.

[9] S.V. Dzyadevych, T.M. Anh, A.P Soldatkin, N.D. Chien, N. Jaffrezic-Renault, J.M. Chovelon, "Development of enzyme biosensor based on pH-sensitive field-effect transistors for detection of phenolic compounds", *Bioelectrochem.*, vol. 55, no. 1-2, pp. 79–81, Jan. 2002.

[10] A.P.Soldatkin, V.N. Arkhypova, S.V. Dzyadevych, V. Anna, J.M. Gravoueille, N. Jaffrezic-Renault, C. Martelet, "Analysis of the potato glycoalkaloids by using of enzyme biosensor based on pH-ISFETs", *Talanta*, vol. 66, no. 1, pp. 28-33, Mar. 2005.

[11] V.-T. Nguyen, Y. S. Kwon, and M. B. Gu, "Aptamer-based environmental biosensors for small molecule contaminants", *Curr. Opin. Biotechnol.*, vol. 45, pp. 15–23, Jun. 2017.

[12] B.A. Makwana, S. Darjee, V.K. Jain, A. Kongor, G. Sindhav, and M.V. Rao, "A comparative study: Metal nanoparticles as fluorescent sensors for biomolecules and their biomedical application", *Sens. Actuators B Chem.*, vol. 246, pp. 686-695, Jul. 2017.

[13] I. Cimalla, F. Will, K. Tonisch, M. Niebelschütz, V. Cimalla, V. Lebedev, G. Kittler, M. Himmerlich, S. Krischok, J.A. Schaefer, and M. Gebinoga, "AlGaN/GaN biosensor—effect of device processing steps on the surface properties and biocompatibility", *Sens. Actuators B Chem.*, vol. 123, no. 2, pp. 740-748, May 2007.

[14] T. Kokawa, T. Sato, H. Hasegawa, and T. Hashizume, "Liquid-phase sensors using open-gate AlGaN/GaN high electron mobility transistor structure", *J. Vac. Sci. Technol., B: Microelectron. Nanometer Struct. Process., Meas., Phenom.*, vol. 24, no. 4, pp. 1972-1976, Jul. 2006.

[15] R. Thapa, S. Alur, K. Kim, F. Tong, Y. Sharma, M. Kim, C. Ahyi, J. Dai, J. Wook Hong, M. Bozack, and J. Williams, "Biofunctionalized AlGaN/GaN high electron mobility transistor for DNA hybridization detection", *Appl. Phys. Lett.*, vol. 100, no. 23, Art. no. 232109, Jun. 2012.

[16] R. Ajay, M. Narang, M. Saxena, and M. Gupta, "Model of GaSb-InAs p-i-n Gate All Around BioTunnel FET", *IEEE Sens. J*, vol. 19, no. 7, pp. 2605–2612, Dec. 2019.

[17] K. Boucart, W. Riess and A.M. Ionescu, "Lateral strain profile as key technology booster for all-silicon tunnel FETs", *IEEE Electron Device Lett.*, vol. 30, no. 6, pp. 656-658, Apr. 2009.

[18] K Boucart and A.M. Ionescu, "Double-gate tunnel FET with high-κ gate dielectric", *IEEE Trans. on Electron Devices*, vol. 54, no. 7, pp. 1725-1733, Jun. 2007.

[19] W.Y. Choi, B.G. Park, J.D. Lee and T.J.K. Liu, "Tunneling field-effect transistors (TFETs) with subthreshold swing (SS) less than 60 mV/dec", *IEEE Electron Device Lett.*, vol. 28, no. 8, pp. 743-745, Jul. 2007.

[20] S. Saurabh and M.J. Kumar, "Novel attributes of a dual material gate nanoscale tunnel field-effect transistor", *IEEE Trans. on Electron Devices*, vol. 58, no. 2, pp. 404-410, Dec. 2010.

[21] C. Sandow, J. Knoch, C. Urban, Q. T. Zhao, S. Mant, "Impact of electrostatics and doping concentration on the performance of silicon tunnel field-effect transistors", *Solid State Electron.*, vol. 53, no. 10, pp. 1126–1129, Oct. 2009.

[22] J. Min, J. Wu, Y. Taur, "Analysis of source doping effect in tunnel FETs with staggered bandgap", *IEEE Electron Device Lett.*, vol. 34, no. 10, pp. 1094–1096, Aug. 2015.

[23] C. Convertino, H. Schmid, L. Czornomaz, H. Riel, S. Sant, A. Schenk, and K. Moselund, "Complementary III-V heterojunction tunnel FETs monolithically integrated on silicon", *ECS Trans.*, vol. 85, no. 6, Art. no. 139, Apr. 2018.

[24] K.K. Bhuwalka, S. Sedlmaier, A.K. Ludsteck, C. Tolksdorf, J. Schulze, and I. Eisele, "Vertical tunnel field-effect transistor", *IEEE Trans. Electron Devices*, vol. 51, no. 2, pp. 279-282, Jan. 2004.

[25] A. Anam, S. Anand and S. I. Amin, "Design and Performance Analysis of Tunnel Field Effect Transistor with Buried Strained $Si_{1-x}Ge_x$ Source Structure Based Biosensor for Sensitivity Enhancement", *IEEE Sens. J*, vol. 20, no. 22, pp. 13178-13185, Jun. 2020.

[26] S. Kumar, Y. Singh, B. Singh and P. K. Tiwari, "Simulation Study of Dielectric Modulated Dual Channel Trench Gate TFET Based Biosensor", *IEEE Sens. J*, vol. 20, no. 21, pp. 12565-12573, Jun. 2020.

[27] S. Kanungo, B. Majumdar, S. Mukhopadhyay, D. Som, S. Chattopadhyay and H. Rahaman, "Investigation on the Effects of Substrate, Back-Gate Bias and Front-Gate Engineering on the Performance of DMTFET-Based Biosensors", *IEEE Sens. J*, vol. 20, no. 18, pp. 10405-10414, May 2020.

[28] S. Ghosh, A. Chattopadhyay and S. Tewari, "Optimization of Hetero- Gate-Dielectric Tunnel FET for Label-Free Detection and Identification of Biomolecules", *IEEE Trans. Electron Devices*, vol. 67, no. 5, pp. 2157-2164, Mar. 2020.

[29] K. Tomioka, J. Motohisa, S. Hara and T. Fukui, "Control of InAs nanowire growth directions on Si", *Nano Lett.*, vol. 8, no. 10, pp. 3475-3480, Oct. 2008.

[30] K.E. Moselund, D. Cutaia, H. Schmid, M. Borg, S. Sant, A. Schenk, and H. Riel, "Lateral InAs/Si p-type tunnel FETs integrated on Si-part 1: experimental devices", *IEEE Trans. Electron Devices*, vol. 63, no. 11, pp. 4233-4239, Oct. 2016.

[31] J.S. Michaelson, E. Halpern, and D.B. Kopans, "Breast cancer: computer simulation method for estimating optimal intervals for screening", *Radiology*, vol. 212, no. 2, pp. 551-560, Aug. 1999.

[32] K. Tomioka, M. Yoshimura and T. Fukui, "Vertical $In_{0.7}Ga_{0.3}As$ nanowire surrounding-gate transistors with high-k gate dielectric on Si substrate", *Int. Electron Devices Meet.*, pp. 33-3, Dec. 2011.

[33] K. Tomioka, M. Yoshimura and T. Fukui, "A III–V nanowire channel on silicon for high-performance vertical transistors", *Nature*, vol. 488, no. 7410, pp. 189-192, Aug. 2012.

[34] S. Sant, K. Moselund, D. Cutaia, H. Schmid, M. Borg, H. Riel, and A. Schenk, "Lateral InAs/Si p-type tunnel FETs integrated on Si—Part 2: Simulation study of the impact of interface traps", *IEEE Trans. Electron Devices*, vol. 63, no. 11, pp. 4240-4247, Oct. 2016.

[35] Z. Mitri, T. Constantine, and R. O'Regan, "The HER2 receptor in breast cancer: Pathophysiology, clinical use, and new advances in therapy", *Chemother Res Pract.*, Art. no. 743193, Dec. 2012.

[36] H. J. Burstein, "The distinctive nature of HER2-positive breast cancers", *N. Engl. J. Med.*, vol. 353, no.16, pp. 1652-1654, Oct. 2005.

[37] G. Wadhwa and B. Raj, "Parametric variation analysis of symmetric double gate charge plasma JLTFET for biosensor application", *IEEE Sens. J*, vol. 18, no. 15, pp. 6070-6077, Jun. 2018.

[38] S. Singh, P.N. Kondekar and N.K. Jaiswal, "Label-free biosensor using nanogap embedded dielectric modulated schottky tunneling source impact ionization MOS", *Microelectron. Eng.*, 149, pp. 129-134, Jan. 2016.

[39] G. Wadhwa and B. Raj, "Label free detection of biomolecules using charge-plasma-based gate underlap dielectric modulated junctionless TFET", *J. Electron. Mater.*, vol. 47, no. 8, pp. 4683-4693, Aug. 2018.

[40] G. Wadhwa and B. Raj, "Design, simulation and performance analysis of JLTFET biosensor for high sensitivity", *IEEE Trans. Nanotechnol.*, vol. 18, pp. 567-574, May 2019.

[41] S. Singh, P.N. Kondekar, and N.K. Jaiswal, "Comparative Analysis of T-Gate and L-Gate Dielectric Modulated Schottky Tunneling Source Impact Ionization MOS for Label-Free Detection of Toxic Gases", *J. Nanoelectron. Optoelectron.*, vol. 13, no. 4, pp. 501-508, Apr. 2018.

[42] S. Mukhopadhyay, D. Sen, B. Goswami, and S.K. Sarkar, "Performance Evaluation of Dielectrically Modulated Extended Gate Single cavity InGaAs/Si HTFET based Label-free Biosensor Considering Non-ideal Issues", *IEEE Sens. J*, vol. 21, no. 4, pp. 4739-4746, Oct. 2020.

[43] M. Johansson, I. Lundström, and L. G. Ekedahl, "Bridging the pressure gap for palladium metal-insulator-semiconductor hydrogen sensors in oxygen containing environments", *J. Appl. Phys.*, vol. 84, no. 1, pp. 44-51, Jul. 1998.

[44] K.H. Chen, B.S. Kang, H.T. Wang, T.P. Lele, F. Ren, Y.L. Wang, C.Y. Chang, S.J. Pearton, D.M. Dennis, J.W. Johnson, and P. Rajagopal, "C-erbB-2 sensing using AlGaN/GaN high electronmmobility transistors for breast cancer detection", *Appl. Phys. Lett.*, vol. 19, no. 3, Art. no. 57, May 2009.

[45] M. Barbaro, A. Bonfiglio, L. RaffoL, "A charge-modulated FET for detection of biomolecular processes: conception, modeling, and simulation", *IEEE Trans. Electron Devices*, vol. 53, no. 1, pp. 158-166, Dec. 2005.

[46] G. Koblmueller, and G. Abstreiter, "Growth and properties of InGaAs nanowires on silicon", *Phys Status Solidi Rapid Res Lett.*, vol. 8, no. 1, pp. 11-30, Jan. 2014.

[47] ATLAS Device Simulation Software, Silvaco Int., Santa Clara, CA, USA, 2014.

[48] K.H. Chen, B.S. Kang, H.T. Wang, T.P. Lele, F. Ren, Y.L. Wang, C.Y. Chang, S.J. Pearton, D.M. Dennis, J.W. Johnson, and P. Rajagopal, "C-erbB-2 sensing using AlGaN/Ga N high electron mobility transistors for breast cancer detection", *Appl. Phys. Lett.*, vol. 92, no. 19, Art. no. 192103, May 2008.

[49] A. Ould-Abbas, O. Zeggai, M. Bouchaour, H. Zeggai, N. Sahouane, M. Madani, D. Trari, M. Boukais, and N.E. Chabane-Sari, N.E., 2013. Study on functionalizing the surface of AlGaN/GaN high electron mobility transistor based sensors", *J. Optoelectron. Adv. Mater.*, vol. 15, pp. 1323-1327, Nov. 2013.

[50] S. Vasudevan, K. Walczak, N. Kapur, M. Neurock, and A. W. Ghosh, "Modeling electrostatic and quantum detection of molecules", *IEEE Sens. J*, vol. 8, no.6, pp. 857–862, May 2008.

[51] A. Varghese, C. Periasamy, and L. Bhargava, "Analytical modeling and simulation-based investigation of AlGaN/AlN/GaN Bio-HEMT sensor for C-erbB-2 detection", *IEEE Sens. J*, vol. 18, no. 23, pp. 9595-9603, Sep. 2018.

[52] T. Li, R. P. Joshi, and R. D. del Rosario, Requirements for low inter modulation distortion in GaN-$Al_xGa_{1-x}N$ high electron mobility transistors: A model assessment, *IEEE Trans. Electron Devices*, vol. 49, no. 9, pp. 1511-1518, Nov. 2002.

[53] H. Ilatikhameneh, "Steep Sub-Threshold Swing Transistors", Doctoral dissertation, Purdue University, West Lafayette, *Indiana*, 2017.

[54] M. Verma, S. Tirkey, S. Yadav, D. Sharma, and D. S. Yadav, "Performance assessment of a novel vertical dielectrically modulated TFET-based biosensor", *IEEE Trans. Electron Devices*, vol. 64, no. 9, pp. 3841–3848, Sep. 2017.

[55] V.D. Wangkheirakpam, B. Bhowmick, and P.D. Pukhrambam, "N^+ Pocket Doped Vertical TFET Based Dielectric-Modulated Biosensor Considering Non-Ideal Hybridization Issue: A Simulation Study", *IEEE Trans. Nanotechnol.*, vol. 19, pp. 156-162, Jan. 2020.

[56] H. Im, X. Huang, B. Gu, and Y. Choi, "A dielectric-modulated field effect transistor for biosensing", *Nat. Nanotechnol.*, vol. 2, no. 7, pp. 430–434, Jul. 2007.

[57] S. Kanungo, S. Chattopadhyay, P.S. Gupta, and H. Rahaman, "Comparative performance analysis of the dielectrically modulated full gate and short-gate tunnel FET-based biosensors", *IEEE Trans. Electron Devices*, vol. 62, no. 3, pp. 994–1001, Feb. 2015.

[58] D. Sarkar, and K. Banerjee, "Proposal for tunnel-field-effect- transistor as ultra-sensitive and label-free biosensors", *Appl. Phys. Lett.*, vol. 100, no. 14, Art. no. 143108-1-4, Apr. 2012.